soil systems

MDPI

Article

Reduction of Birnessite as Influenced by Iron(II) and Salicylate

Jonathan L. Edwards and Christopher J. Matocha *

Plant and Soil Sciences, University of Kentucky, Lexington, KY 40546, USA; jledwards@uky.edu
* Correspondence: cjmato2@uky.edu

Abstract

Manganese (III,IV) (hydr) oxide minerals, and especially birnessite, have long been identified as important sorbents and oxidants of metals and metalloids in soil and sediment environments. Although the oxidation of dissolved ferrous iron (Fe(II)) concurrent with hexagonal birnessite reduction has been recognized for quite some time, fundamental kinetic data are lacking. In addition, the role of dissolved organic carbon (DOC) in affecting this process is unknown. In this study, stirred-batch kinetic experiments involving hexagonal birnessite reduction and dissolved Fe(II) removal were performed under anoxic conditions at pH 4 and 10° C in the presence and absence of salicylate as a model ligand for DOC. The reaction with Fe(II)-only shows a first-order dependence on both initial dissolved Fe(II) and effective birnessite surface site concentration, with an overall second-order rate coefficient (k) of $4.54 \times 10^{-3} \pm 8.6 \times 10^{-4}$ L m^{-2} min^{-1}. The addition of salicylate to Fe(II) solutions increased the initial rate of dissolved Mn(II) production by 9.5- ($p = 0.006$) and 7-fold ($p < 0.001$) when compared with identical Fe(II)-only treatments. This is likely due in part to the effect of salicylate on the redox potential of the Fe(II)-Fe(III) couple. This study provides further insight into the role of birnessite in Fe(II) oxidation.

Keywords: manganese; iron; birnessite; sorption; complexation; salicylate; electron transfer

1. Introduction

Manganese (Mn) (III,IV) (hydr) oxide minerals can chemically oxidize iron(Fe(II)) that has diffused in from Fe(III)-reducing zones or where Mn(III,IV)- and Fe(III)-reducing zone overlap [1–5]. Environments where this process has been shown to be important include marine sediments, freshwater aquifers bounded by fresh and saline water, contaminated aquifers, and highly weathered field soils [1,3,5,6]. In order to successfully predict the concentration profiles of Fe(II) and Mn(II) in porewater, reactive transport models have incorporated kinetic expressions involving the heterogeneous oxidation of dissolved Fe(II) oxidation by Mn(III,IV) (hydr) oxide minerals [1,2]. This process can account for as much as 75% of the Mn(IV) reduced in marine sediments [1].

Fundamental kinetic studies of Mn (III,IV) (hydr) oxide mineral reduction by dissolved Fe(II) have focused on either monoclinic birnessite, polymeric MnO_2, or tunnel structures such as pyrolusite. For example, Postma [7] studied the reductive dissolution of a monoclinic birnessite by dissolved Fe(II) between pH 3–6 at 10 °C. At pH 3, the kinetics of birnessite reduction were rapid while a noticeable decrease occurred at pH $\geq$ 4 due to the production of a Fe(III) hydroxide mineral as Fe(II) was oxidized. The reductive dissolution rate of birnessite based on dissolved Mn(II) production exhibited a first-order dependence on birnessite surface sites. Villinski and coworkers [8,9] reported that reduction of a pyrolusite-coated quartz sand by dissolved Fe(II) was inhibited as Fe(III)

Check for updates

Academic Editor: Richard Wilkin

Received: 29 July 2026
Revised: 24 September 2026
Accepted: 5 October 2026
Published: 9 October 2026

Copyright: © 2026 by the authors. Licensee MDPI, Basel, Switzerland. This article is an open access article distributed under the terms and conditions of the Creative Commons Attribution (CC BY) license.

precipitated. Using polymeric MnO_2, Siebecker et al. [10] noted a first-order dependence on both dissolved Fe(II) and MnO_2 concentrations with a large second-order rate constant. Burdige et al. [11] showed that the nature of the Mn oxide mineralogy made a difference in the reactivity with respect to Fe(II) oxidation, with triclinic birnessite reacting more quickly than pyrolusite. To our knowledge, no fundamental rate equation exists describing hexagonal birnessite reduction by dissolved Fe(II), although numerous studies note the rapid nature of this reaction [12–17]. This is surprising in light of the fact that hexagonal birnessite is one of the most commonly identified Mn oxide minerals [18–20].

The microbial reduction of Fe(III) to Fe(II) is facilitated by the presence of soil organic carbon [21]. Thus, in anoxic environments, solution Fe(II) and dissolved organic carbon (DOC) are likely to co-exist and this has been reported in wetlands, where levels can exceed 1 mM Fe(II) and 3 mM DOC, respectively [22]. The complexation of dissolved Fe(II) by organic ligands in solution with oxygen as the ligating atom strongly enhances its reactivity with respect to hexaaquo Fe(II) [23,24]. For example, dissolved Fe(II)–organic complexes were reported to accelerate reduction in solid-phase Fe(III) oxide minerals [25] and chromate [26] to produce dissolved Fe(III) complexes. It is conceivable that Mn(III,IV) (hydr) oxide minerals could react with dissolved Fe(II)–organic complexes where Mn(III,IV)- and Fe(III)-reducing zones overlap in anoxic porewater [27]. However, to our knowledge, the reactivity of dissolved Fe(II) in the presence of dissolved organics with Mn(III,IV) (hydr) oxide minerals has not been studied.

The objective of this study was to collect fundamental kinetic data on Fe(II) removal by hexagonal birnessite in the presence and absence of a well-defined organic compound (salicylate). Salicylate was selected as the model organic ligand because it represents a low-molecular-weight aromatic acid that has been identified in DOC [28] and has been shown to accelerate chromium(VI) reduction by dissolved Fe(II) [26].

2. Materials and Methods

2.1. Birnessite Synthesis and Characterization

Birnessite was prepared by reducing potassium permanganate ($KMnO_4$) with concentrated hydrochloric acid (HCl), as described elsewhere [29]. The resulting particles were dialyzed in deionized water using dialysis tubing and freeze-dried. The particles were characterized by x-ray diffraction (XRD) using a Bruker AXS D8 Discover Diffractometer (Billerica, MA, USA) with CuKα radiation using a 22 s step time and 0.03^0 per step. X-ray diffraction peaks were located at 0.72 nm (d001), 0.36 nm (d002), 0.242 nm (d100), and 0.140 nm (d110) (Figure S1A), consistent with the presence of hexagonal birnessite [19]. The average oxidation state determined by iodometric titration was 3.93 $\pm$ 0.08 (n = 3). The BET surface area of birnessite, measured using a Micromeritics Tristar 3000 gas adsorption analyzer (Malvern Panalytical, Westborough, MA, USA), was 92.7 $m^2\ g^{-1}$. The point of zero salt effect (PZSE) was estimated to occur at a pH of 2.6 $\pm$ 0.1 (n = 3). Scanning electron microscopy showed that birnessite forms submicrometer honeycomb-like interconnected sheet networks (Figure S1B).

2.2. Stirred-Batch Experiments of Fe(II)–Birnessite

Stirred-batch experiments were conducted under anoxic conditions using a constant flow of N_2 purge gas and birnessite suspensions in 10 mM $NaC_2H_3O_2$-$C_2H_4O_2$ (acetate) buffered to pH 4. The stirred-batch reactor was maintained at 10 °C during the reactions to mimic conditions described elsewhere [7] using a VWR circulating water bath (Radnor, PA). Fresh aqueous Fe(II) stock solutions (0.1 M) were prepared in an O_2-free glove box (Coy Laboratory Products, Grass Lake, MI, USA) using $FeCl_2 \cdot 4H_2O$ and deoxygenated deionized water. An aliquot of $FeCl_2$ from a 0.1 M stock solution was added to a prehydrated birnessite

suspension to initiate the reactions. The initial Fe(II) concentration ranged from 250 to 930 μM and effective surface site (*ESS*) concentration of birnessite ranged from 2.78 to 55.62 m^2 L^{-1}. The birnessite suspensions were stirred at 300 rpm using a magnetic stir plate and a Teflon-coated stir bar. Suspension samples were removed at designated time points and filtered through 0.2 μm membrane filters (Fisher Scientific, Hampton, NH, USA). A subsample of the filtrate was immediately mixed with ferrozine (3-(2-pyridyl)-5,6-diphenyl-1,2,4-triazine-4′, 4″-disulfonic acid monosodium salt) and the absorbance of the Fe(II)-ferrozine complex was quantified at 562 nm [30] on a double-beam Shimadzu UV-3101 PC spectrophotometer (Kyoto, Japan) using a quartz cell with a 1 cm pathlength. The cell holder was equipped with a Peltier temperature controller that allowed solutions to be measured at the experimental temperature of 10 °C. The molar absorptivity of the Fe(II)–ferrozine complex was 2.7 $\times 10^4$ M^{-1} cm^{-1}. The ferrozine solutions were also analyzed for total dissolved Mn (Mn_T) using atomic absorption spectrometry (AAS) on a Shimadzu AA-6800 (Kyoto, Japan). The detection limits for Fe(II) and Mn_T were 0.62 micromolar and 1.7 micromolar, respectively.

A sorption isotherm was performed under anoxic conditions to account for resorption of released Mn(II) to unreacted birnessite surface sites [11,31]. A stock solution of Mn(II) was prepared from $MnCl_2$ (0.1 M) and aliquots were added to 40 mL centrifuge tubes containing 0.1 *g* birnessite/L (*ESS* 5.56 m^2 L^{-1}) buffered to pH 4 to achieve initial concentrations of Mn(II) ranging from 25 to 500 μM. Suspensions were shaken for 1 h followed by centrifugation at 8000 rpm and filtration through 0.2 μm membrane filters. Dissolved Mn(II) in equilibrium with birnessite was quantified using AAS, as mentioned above.

The progress of the reductive dissolution of birnessite was monitored by assuming that dissolved Mn_T equals dissolved Mn(II) and following Mn(II) production over time. Initial linear portions of Mn(II) produced as a function of time were fit using linear least squares regression for kinetic analysis [32]. Reactions were performed in triplicate reactors.

2.3. Stirred-Batch Experiments of Fe(II)-Salicylate-Birnessite

The experimental setup to study the effect of salicylate-complexed Fe(II) on the reductive dissolution of birnessite was identical to the birnessite–Fe(II) experiments (pH 4.0 and 10 °C). A stock solution of 0.1 M Fe(II) in 0.5 M Na–salicylate was prepared in the O_2-free glove box. Aliquots of the Fe(II)–salicylate stock solution were added to stirred birnessite suspensions of 0.05 (2.78 m^2 L^{-1}) and 0.1 g L^{-1} (5.56 m^2 L^{-1}) to achieve initial Fe(II) and salicylate concentrations of 930 μM and 5 mM, respectively. This concentration of salicylate was chosen to mimic dissolved organic carbon levels reported in wetland environments [22]. Suspension samples were removed at identical time points as the Fe(II)-alone experiments and filtered through 0.2 micron membrane filters. Filtrates were complexed with ferrozine and treated identically, as described above.

Three types of control bottles were included in the experiments. An experiment was run where Fe(II) was omitted (birnessite-only) to check for possible proton-promoted dissolution of birnessite and another control bottle was run to evaluate the removal of Fe(II) in the absence of birnessite (Fe(II)-only). A third control was run to account for the possible reductive dissolution of birnessite by salicylate alone, where Fe(II) was omitted (birnessite–salicylate).

2.4. Characterization of Fe(II)–Birnessite and Fe(II)–Salicylate–Birnessite Reaction Products

Reaction products were characterized from the Fe(II)-birnessite and Fe(II)–salicylate–birnessite suspensions after 60 min of reaction time at pH 4, 10 °C, 55.6 m^2 L^{-1} birnessite concentration and 930 μM Fe(II) using XRD. Suspensions were filtered onto 0.2 μm membrane filters, which were then taped on glass slides under anoxia and then scanned using a Bruker AXS D8 Discover Diffractometer as described above.

Diffuse reflectance spectroscopy (DRS), a technique which can probe the oxidation state and coordination of transition metals [33,34], was employed to follow the progress of the reductive dissolution of birnessite by dissolved Fe(II). Wet pastes were scanned after 5 min of reaction time between 930 μM dissolved Fe(II) and 5.56 m^2 L^{-1} birnessite at pH 4 and compared with unreacted birnessite. Spectra were collected using a double-beam Shimadzu UV-3101 UV-VIS-NIR spectrophotometer equipped with an ISR 3100 integrating sphere attachment (Kyoto, Japan) from 2000 nm to 200 nm with a 12 nm slit width calibrated against a Spectralon standard.

3. Results and Discussion

3.1. Fe(II)–Birnessite

Dissolved Fe(II) was rapidly removed from solution in the presence of 0.05 g L^{-1} birnessite (corresponding to an effective surface site concentration (*ESS*) of 2.78 m^2 L^{-1}) at pH 4 and this was concurrent with the immediate appearance of dissolved Mn_T, the latter of which we assumed equals dissolved Mn(II) (Figure 1A). A representative control experiment without birnessite (Fe(II)-only) showed little change in Fe(II), ruling out precipitation of incipient Fe(II) solids or Fe(II) oxygenation by trace amounts of oxygen as responsible for removing Fe(II) from solution (Figure S2). Likewise, a control experiment where Fe(II) was omitted (birnessite-only) showed very low levels of Mn(II) being released under these conditions from 2.78 m^2 L^{-1} birnessite suspensions at pH 4.0 (Figure S3). This indicates that the proton-promoted reduction of birnessite did not contribute to Mn(II) release under our experimental conditions.

In order to account for the readsorption of evolved Mn(II) to remaining birnessite surface sites [11,31], which would lower the amount of Mn(II) produced, we separately measured a sorption isotherm of Mn(II) on birnessite. The sorption data yielded a linear isotherm with a distribution coefficient (K_D) of 0.443 μM/μM (Figure S4). Dissolved Mn(II) values were corrected for sorbed Mn(II) and used in subsequent calculations, an approach used elsewhere [11].

The stoichiometry was assessed by plotting Fe(II) concentration versus Mn(II) produced. The slope of the least squares linear regression was Δ[FeII]/[Mn(II)]. The slope value for the 2.78 m^2 L^{-1} birnessite surface site level was −1.95, in agreement with the predicted value of −1.93 based on the average oxidation state for hexagonal birnessite ($Mn^{3.93}O_{1.96\ (s)}$) (Figure 2).

The Fe(II)-reacted birnessite after 60 min of reaction time showed x-ray diffraction peaks corresponding to d-spacings located at 0.73, 0.36, 0.24, and 0.14 nm, which indicated the presence of remaining birnessite (Figure 3). The broad feature between 15 and 40° two theta most likely corresponds to poorly crystalline ferrihydrite ($Fe(OH)_{3(s)}$), which is known to give broad XRD lines in that region. This agrees with past studies, which have shown ferrihydrite to be a product of Fe(II) oxidation by MnO_2 [7–9].

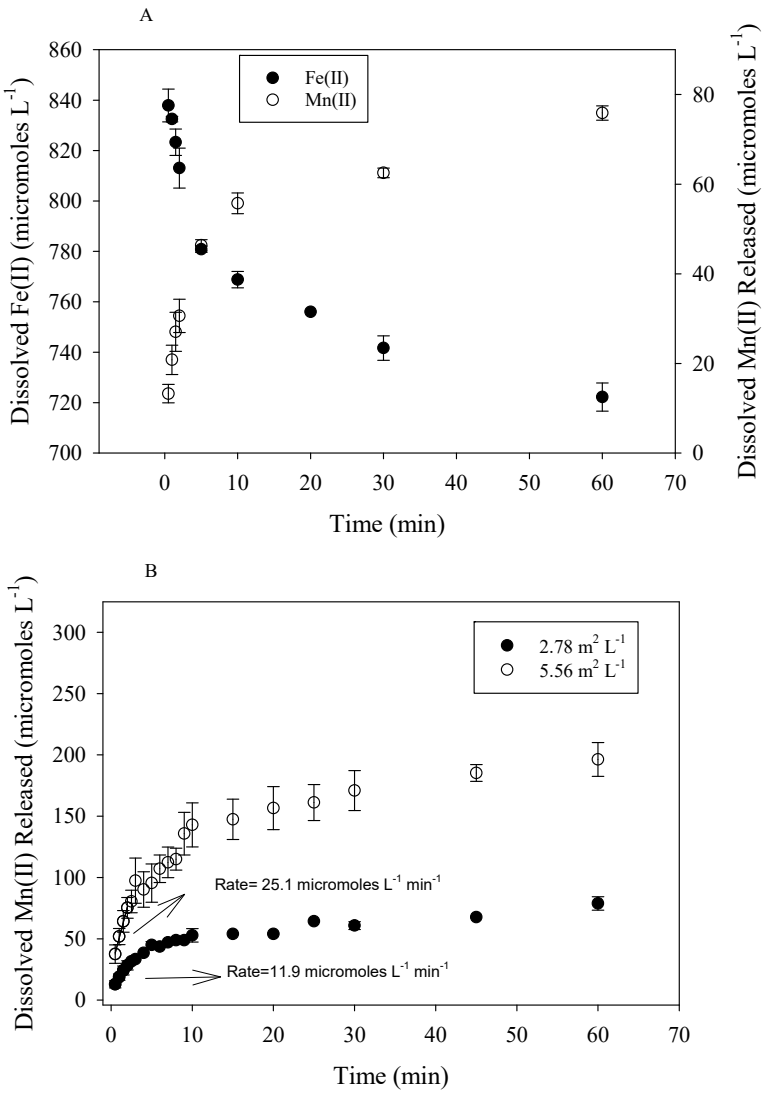


Figure 1. Time course of (**A**) dissolved Fe(II) and Mn(II) for a birnessite effective surface site (*ESS*) concentration of 2.78 m^2 L^{-1} and (**B**) initial rates of dissolved Mn(II) release at 2.78 m^2 L^{-1} and 5.56 m^2 L^{-1} at an initial Fe(II) concentration of 930 micromoles L^{-1}, pH 4, and 10 °C.

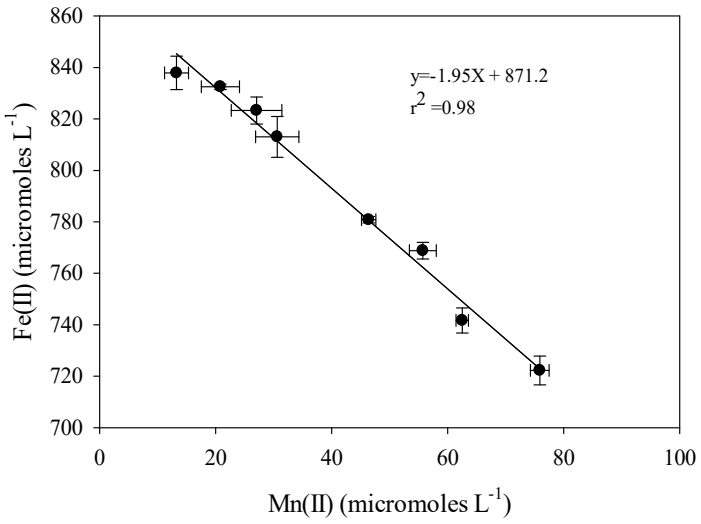


Figure 2. Reaction stoichiometry describing Fe(II) consumed versus Mn(II) released for an *ESS* level of 2.78 m^2 L^{-1}, pH 4, 10 °C, and an initial Fe(II) concentration of 930 micromoles L^{-1}.

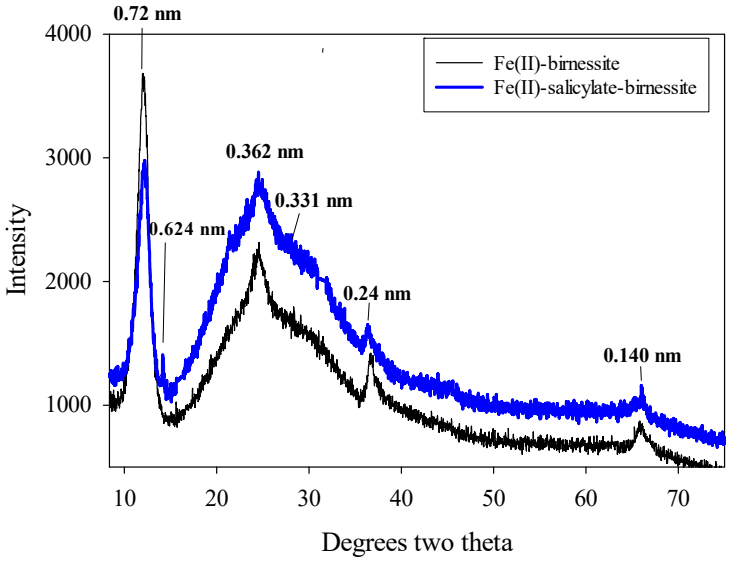


Figure 3. X-ray diffractograms (using Cu K_α radiation) of the Fe(II)–birnessite and Fe(II)–salicylate–birnessite experiment reaction products after 60 min of reaction time, 10 °C, pH 4, 55.6 m^2 L^{-1} birnessite concentration, and an initial Fe(II) concentration of 930 micromoles L^{-1}.

The disappearance of dissolved Fe(II) from solution is attributed to the sorption of Fe(II) followed by its oxidation to solid-phase Fe(III), with concomitant reduction of birnessite to Mn(II). An overall reaction describing dissolved Fe(II) oxidation by birnessite can be written given the average oxidation state for hexagonal birnessite ($Mn^{3.93}O_{1.966\ (s)}$) and ferrihydrite as the solid-phase product.

$$Mn^{3.93}O_{1.966\ (s)} + 1.93Fe^{2+}{}_{(aq)} + 3.83H_2O \rightarrow Mn^{2+}{}_{(aq)} + 1.93Fe(OH)_{3(s)} + 1.87H^+ \quad (1)$$

Separate experiments using a pH-stat to control pH at 4 rather than the buffer showed a consumption of OH^- during this reaction in agreement with Equation (1). This agrees with past research documenting Fe(II) oxidation by hexagonal birnessite [15–17], monoclinic, and triclinic birnessites [7,11].

The kinetics of Mn(II) production were quantified using the initial rate and isolation methods [32] to evaluate the rate expression at pH 4 and 10 °C, as shown below:

$$\frac{d\left[Mn^{2+}_{(aq)}\right]}{dt} = k[ESS]^a\left[Fe^{2+}\right]^b \quad (2)$$

where $\frac{d\left[Mn^{2+}_{(aq)}\right]}{dt}$ is the initial rate of Mn(II) production (μmol L^{-1} min^{-1}), $[ESS]$ is the effective surface site term (m^2 L^{-1}), $\left[Fe^{2+}\right]$ is the concentration of dissolved Fe(II) (μmol L^{-1}), k is the overall reaction rate coefficient (L m^{-2} min^{-1}), and a and b represent the reaction orders with respect to $[ESS]$ and $\left[Fe^{2+}\right]$, respectively. The ESS was calculated by multiplying the specific surface area (m^2 g^{-1}) by the birnessite concentration (g L^{-1}) and a factor of 0.6, the ratio of edge sites to surface sites [35]. The initial linear portion in Mn(II) concentration versus time plots was plotted against the concentration of the reaction component (ESS or Fe^{2+}).

In the presence of excess Fe(II) at a constant pH of 4, the rate expression in Equation (2) can be simplified and expressed with a pseudo-first-order rate coefficient, k_{obs} (min^{-1}):

$$R = \frac{d\left[Mn^{2+}_{(aq)}\right]}{dt} = k_{obs}[ESS]^a \quad (3)$$

where

$$k_{obs} = k\,[Fe^{2+}]^b \quad (4)$$

The initial *ESS* concentration was varied to determine the reaction order using the linearized version of Equation (3):

$$\log\ R\ =\ \log k_{obs} + a \log[ESS] \quad (5)$$

which is shown in Figure 4. Increasing the *ESS* concentration resulted in an increase in the initial rate of dissolved Mn(II) release (Figures 1B and 4). The slope of the log–log plot line is 0.97 ± 0.1, indicating a first-order dependence on *ESS* up to a value of log 1.14 $m^2\ L^{-1}$. This agrees with previous results, where a first-order dependence on monoclinic birnessite and soluble MnO_2 concentrations were reported in reactivity studies with Fe(II) [7,10].

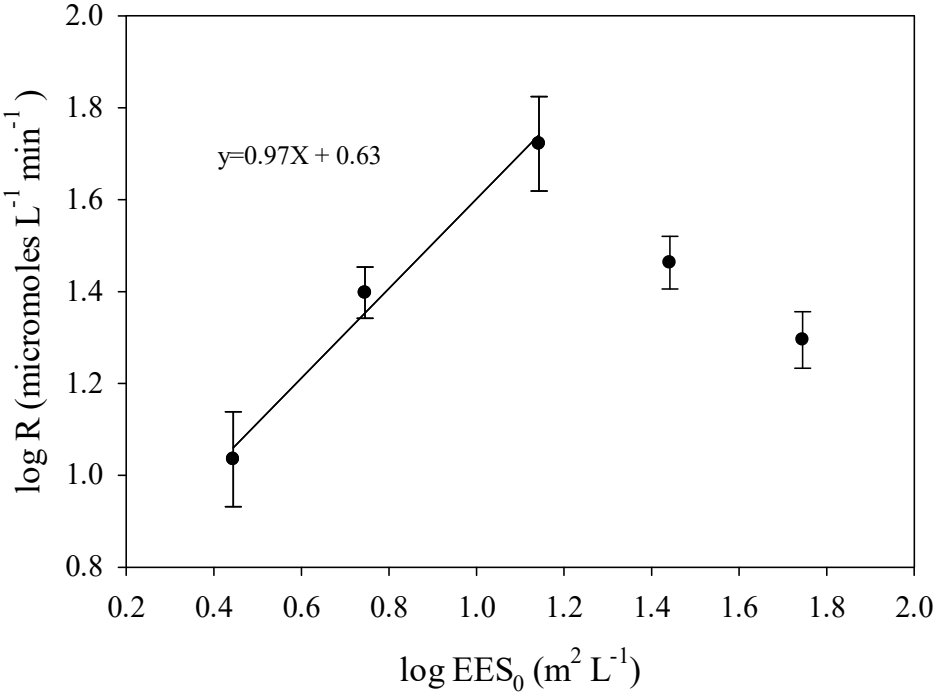


Figure 4. The log of initial rate of dissolved Mn(II) release versus the log of effective surface sites (ESS_0) of birnessite at an initial Fe(II) concentration of 930 micromoles L^{-1}, pH 4, and 10 °C.

The deviation from first-order behavior at the two highest birnessite concentrations, where the initial rate of Mn(II) production decreased with *ESS* level (Figure 4), might be due to enhanced resorption of the released Mn(II) at the two highest birnessite levels (27.8 (log 1.44) and 55.6 (log 1.75) $m^2\ L^{-1}$). This would not be reflected by the isotherm-corrected values at the 5.56 $m^2\ L^{-1}$ level. If the sorption distribution coefficient (K_D) was greater than 0.443 μM/μM (see Figure S4), then one would predict more surface Mn(II) was released from Fe(II) oxidation. In other words, our Mn(II)-corrected values would underpredict reductive dissolution of birnessite. The reaction of dissolved Mn(II) with birnessite occurs on millisecond time scales [36]; thus, it might compete with Fe(II) for reactive surface sites.

To determine the order of the reaction with respect to initial dissolved Fe(II) concentration, the effect of varying the initial Fe(II) concentration at pH 4.0 was evaluated in the presence of an *ESS* level of 2.78 $m^2\ L^{-1}$. The slope of the log–log plot of R versus Fe(II) was 1.1, indicating a first-order dependence on initial Fe(II) concentration (Figure 5). This agrees with the first-order dependence on Fe(II) utilizing polymeric MnO_2 [10].

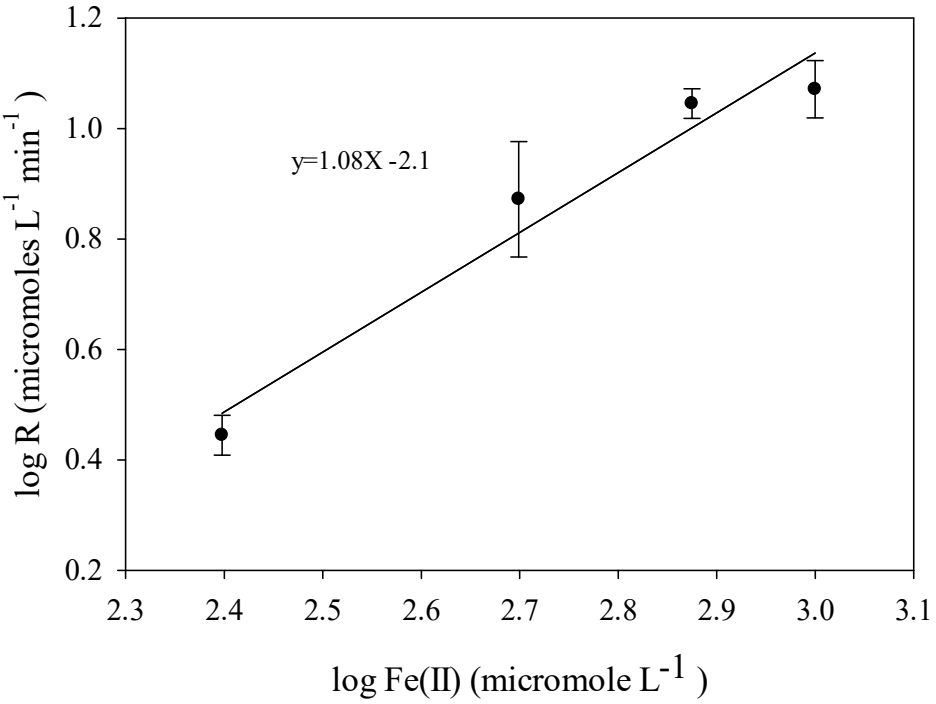


Figure 5. The log of initial rate of dissolved Mn(II) release versus the log of initial Fe(II) concentrations at an initial *ESS* level of 2.78 m^2 L^{-1} birnessite at a pH 4 and 10 °C.

Thus, the oxidation of Fe(II) by birnessite was first-order in both initial Fe(II) and effective surface site concentration, following a second-order rate expression at pH 4 and 10 °C:

$$\frac{d\left[Mn^{2+}_{(aq)}\right]}{dt} = k[ESS]^{1.0}\,[Fe^{2+}]^{1.0} \quad (6)$$

An average rate coefficient, k, was calculated from each experimental run utilizing the rate expression and initial reaction rates. The k value was $4.54 \times 10^{-3} \pm 8.6 \times 10^{-4}$ L m^{-2} min^{-1}, corresponding to a value of 0.37 ± 0.2 L mol^{-1} s^{-1}. This value is comparable to Fe(II) oxidation by pyrolusite [9] and exceeds that of Van Cappellen and Wang [1] (Table 1). The much larger rate coefficient measured by Siebecker et al. [10] might be due to the fact that the soluble MnO_2 employed would have no surface area constraint, leading to more rapid kinetics.

Table 1. Rate coefficients (k) from the literature describing Fe(II) oxidation by Mn oxides.

k	Units	References
0.095	L/mol s	[1] Van Cappellen and Wang, 1996
0.65	L/mol s	[9] Villinski et al., 2003
4338	L/mol s	[10] Siebecker et al., 2015
0.37	L/mol s	This study

The first step in the overall oxidation of dissolved Fe(II) by hexagonal birnessite at pH 4 is sorption of incoming Fe(II) to surface sites on birnessite, forming a precursor surface complex [10,24]. Considering that birnessite has a negative surface charge for pH < 3, favorable electrostatic interactions exist for the Fe(II) cation to form a precursor surface complex. Edge sites are available for cations to sorb on hexagonal birnessite [37]. Hexaaquo Fe(II) has a rapid water-exchange rate, allowing it to rapidly exchange water for surface ligand (oxo) groups on birnessite [24]. Precursor surface complex formation is

followed by electron transfer between the sorbed Fe(II) and either Mn(III) or Mn(IV) sites on the birnessite surface. Frontier molecular orbital theory would predict an inner-sphere mechanism, whereby the electron-donating orbital from Fe(II) with π-type symmetry (t_{2g}^4) would overlap with filled p orbitals of surface oxygen groups on birnessite as a bridging ligand, and would then be transferred to the vacant electron-accepting orbitals of σ^* symmetry (e_g^1 for Mn(III) and e_g^0 for Mn(IV)) [10,24,38,39].

The diffuse reflectance spectra (DRS) of unreacted, hydrated birnessite showed the presence of an intense broad band centered near 20,000 cm^{-1}, which is likely a combination of overlapping peaks (Figure 6). There is also a subtle shoulder near 13,500 cm^{-1}. One of the peaks contributing to the high-energy feature is likely ascribed in part to d-d transitions of Mn(IV), which have been reported near 21,300 cm^{-1} [40]. The shoulder near 13,500 cm^{-1} is likely due to the d-d transition of Mn(III) in a Jahn–Teller tetragonally distorted field [41] and it increases in intensity after 5 min of reaction time with Fe(II). This suggests that Mn(III) is forming as an intermediate during the reduction of birnessite by Fe(II). The oxidation of a second sorbed Fe(II) cation would be necessary to produce Mn(II), which would then be released from the surface in the last step.

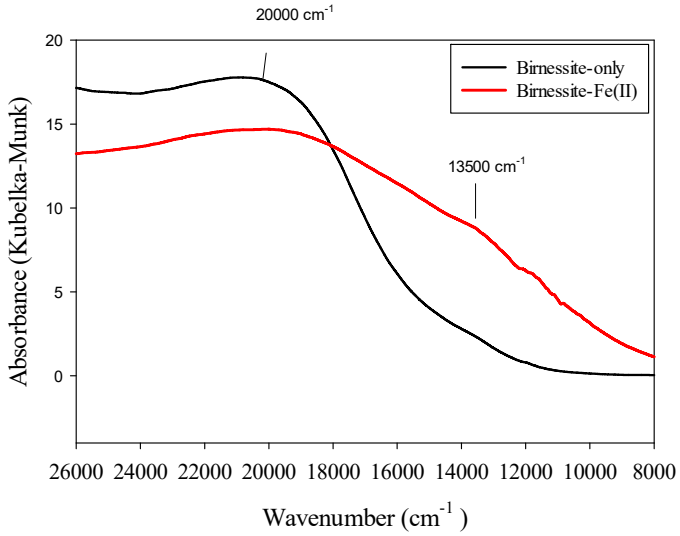


Figure 6. Diffuse reflectance spectra of unreacted birnessite compared with Fe(II)–birnessite after 5 min of reaction time at an initial *ESS* level of 5.56 m^2 L^{-1}, at an initial Fe(II) concentration of 930 micromoles L^{-1}, pH 4, and 10 °C.

3.2. Fe(II)–Salicylate–Birnessite

The addition of salicylate to dissolved Fe(II) solutions resulted in an increase in the reductive dissolution rate of hexagonal birnessite. For example, the initial rates of Mn(II) production were 9.5- ($p = 0.006$) and 7-fold ($p < 0.001$) greater for Fe(II)–salicylate treatments when compared with Fe(II)-only at identical effective surface site concentrations (2.78 m^2 L^{-1} and 5.56 m^2 L^{-1}) (compare Figures 1 and 7). Control experiments with salicylate–birnessite alone showed very limited Mn(II) release (Figure S3), suggesting that salicylate enhances the reductive capacity of dissolved Fe(II).

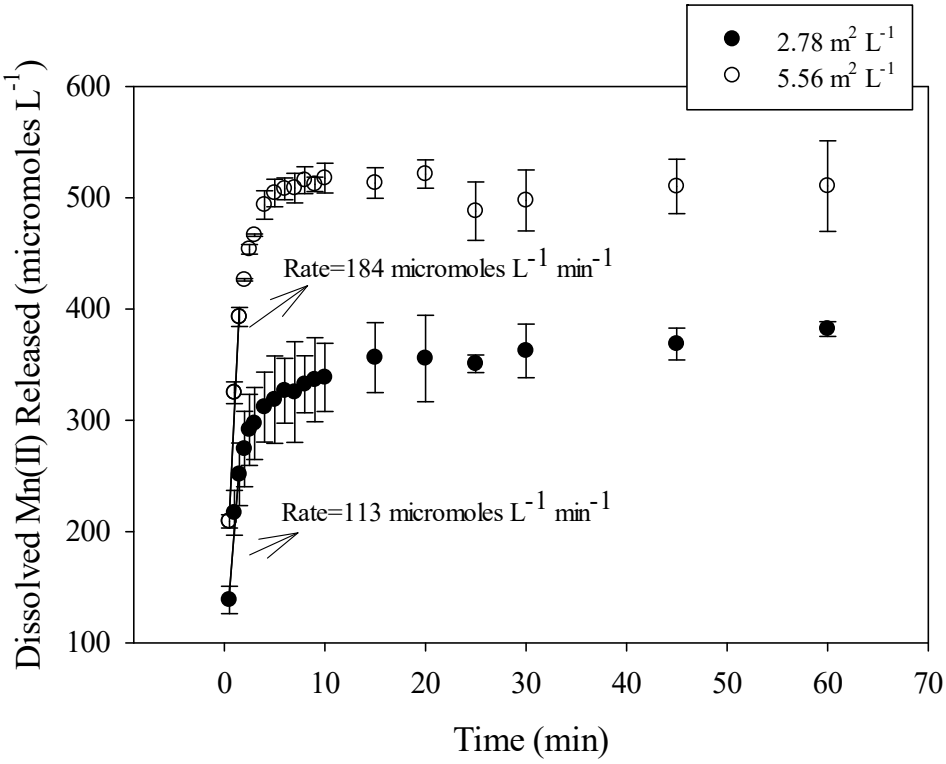


Figure 7. Time course of dissolved Mn(II) release in the presence of 930 micromoles L^{-1} Fe(II), 5 mM salicylate, and *ESS* concentrations of 2.78 m^2 L^{-1} and 5.56 m^2 L^{-1} at pH 4 and 10 °C. Initial rates of Mn(II) release were determined using linear least squares regression.

At identical effective surface site concentrations (55.6 m^2 L^{-1}), Fe(II)–salicylate led to the production of not only poorly crystalline ferrihydrite ($Fe(OH)_3$ but lepidocrocite as well, based on XRD peaks at 0.629 nm and 0.331 nm after 60 min of reaction time (Figure 3). This agrees with Golden et al. [42], where lepidocrocite formation was reported after Fe(II) reacted with triclinic birnessite. In our experiments, there was also a lowered intensity of the parent birnessite peaks at 0.72 nm and 0.36 nm when compared with Fe(II)-only. These findings point to a greater reduction of birnessite by Fe(II)–salicylate solutions when compared with Fe(II)-only.

The acceleration of birnessite reduction by Fe(II)–salicylate solutions when compared with dissolved Fe(II)-only can be rationalized on the basis of the effect of salicylate on the one-electron reduction potential ($E_h{}^0$) of the Fe(III)/Fe(II) couple. The standard $E_h{}^0$ value of the Fe(III)/Fe(II) couple is 0.77 V [23,24]. Salicylate is a bidentate, weak-field ligand with oxygen as the ligating atom. This attribute of salicylate allows it to stabilize the Fe(III) oxidation state, making Fe(II) a better reductant by pushing electron density through the pi molecular orbital system [23,24,43,44]. Complexation by salicylate lowers the reduction potential $\left(E_h^0\right)$ for the Fe(III)/Fe(II) couple, which can be calculated using the following expression [44]:

$$E_h^0 = 0.77 - \frac{RT}{F}\ln\left(\frac{K_{Fe(III)}}{K_{Fe(II)}}\right) \quad (7)$$

where R is the universal gas constant (8.314 J/mol K), T is absolute temperature (K), F is the Faraday constant (96,485 Coulombs/mol) and K is the stability constant describing complexation. Using the stability constants obtained from the MINEQL+ database, it was found that the E_h^0 values were 0.15 V and −0.22 V for the mono-Fe(III)-$(salicylate)_{(aq)}{}^+$/Fe(II)-$(salicylate)_{(aq)}{}^0$ and bis-Fe(III)-$(salicylate)_{2\,(aq)}{}^-$/Fe(II)-$(salicylate)_{2\,(aq)}{}^{2-}$ complexes, respectively. Less positive E_h^0 values brought about by salicylate complexation would make the oxidation of Fe(II) by birnessite more thermodynamically favorable. This would lead to

enhanced reactivity and may explain the dramatic increase in Mn(II) production. It is also possible that there are soluble Mn(III)–salicylate complexes which form and contribute to the dissolved Mn_T pool [24], which awaits experimental confirmation. Our results are consistent with previous work where Cr(VI) reduction rates by Fe(II)–salicylate complexes were several orders of magnitude greater than Fe(II) alone [26].

4. Conclusions

The reduction of hexagonal birnessite through the oxidation of dissolved Fe(II) readily occurred at pH 4 and 10 °C, following a second-order rate expression under anoxic conditions. The second-order rate coefficient was $4.54 \times 10^{-3} \pm 8.6 \times 10^{-4}$ L m^{-2} min^{-1}. The addition of salicylate to dissolved Fe(II) solutions accelerated the birnessite reduction several-fold, attributed to the decrease in the reduction potential of the Fe(III)/Fe(II) couple due to salicylate complexation. Future research would be useful to elucidate the reaction mechanism of this heterogeneous redox reaction.

The results of this study have important implications. The process of reductive dissolution of Mn(III,IV) oxide minerals by dissolved Fe(II) has been shown to occur in environments where dissolved Mn(II) and Fe(II) profiles overlap in marine sediments, accounting for as much as three fourths of the overall Mn(III,IV) reduction while the remainder was attributed to microbial reduction [1]. Madison et al. [45] reported this process to be operative at three of the four stations where porewater chemistry was monitored in near surface marine sediments. It might also be important in surface soils subjected to anoxic conditions, where Mn(II) production was still occurring when dissolved Fe(II) appeared [27,46]. If dissolved organic carbon is produced under these conditions with functional groups which stabilize Fe(III), then the birnessite reduction will be facilitated.

Supplementary Materials: The following supporting information can be downloaded at: https://www.mdpi.com/article/10.3390/soilsystems10100119/s1, Figure S1 Characterization of the synthesized birnessite by x-ray diffraction (A) and scanning electron microscopy (B), Figure S2 A control experiment involving dissolved Fe(II) in the absence of birnessite (Fe(II)-only) at pH 4 and 10 °C, Figure S3 Control experiments involving birnessite-only and birnessite-salicylate at an effective surface site concentration (*ESS*) of 2.78 m^2 L^{-1}, pH 4, and 10 °C, and Figure S4 Isotherm describing Mn(II) sorption by birnessite (5.56 m^2 L^{-1}) at pH 4. The line represents a linear least-squares fit to the data.

Author Contributions: Conceptualization, J.L.E. and C.J.M.; methodology, J.L.E. and C.J.M.; validation, C.J.M.; formal analysis, C.J.M.; investigation, J.L.E. and C.J.M.; data curation, J.L.E. and C.J.M.; writing—original draft preparation, J.L.E. and C.J.M.; writing—review and editing, C.J.M.; supervision, C.J.M.; project administration, C.J.M.; funding acquisition, C.J.M. All authors have read and agreed to the published version of the manuscript.

Funding: This research was supported by National Research Initiative Competitive Grant no. 2002-35107-12214 from the USDA Cooperative State Research, Education, and Extension service.

Data Availability Statement: Data will be made available upon request.

Acknowledgments: We thank Gary Jacobs at the UK Center for Applied Energy for BET analysis of the birnessite, and A.D. Karathanasis and Jason Backus for assistance with XRD.

Conflicts of Interest: The authors declare no conflicts of interest.

References

1. Van Cappellen, P.; Wang, Y. Cycling of iron and manganese in surface sediments; a general theory for the coupled transport and reaction of carbon, oxygen, nitrogen, sulfur, iron, and manganese. *Am. J. Sci.* **1996**, *296*, 197–243. [CrossRef]
2. Smith, S.L.; Jaffé, P.R. Modeling the transport and reaction of trace metals in water-saturated soils and sediments. *Water Resour. Res.* **1998**, *34*, 3135–3147. [CrossRef]
3. Snyder, M.; Taillefert, M.; Ruppel, C. Redox zonation at the saline-influenced boundaries of a permeable surficial aquifer: Effects of physical forcing on the biogeochemical cycling of iron and manganese. *J. Hydrol.* **2004**, *296*, 164–178. [CrossRef]
4. Lovley, D.R.; Phillips, E.J. Manganese inhibition of microbial iron reduction in anaerobic sediments. *Geomicrobiol. J.* **1988**, *6*, 145–155. [CrossRef]
5. Stollenwerk, K.G. Geochemical interactions between constituents in acidic groundwater and alluvium in an aquifer near Globe, Arizona. *Appl. Geochem.* **1994**, *9*, 353–369. [CrossRef]
6. Asghar, M.; Kanehiro, Y. The fate of applied iron and manganese in an oxisol and an ultisol from Hawaii. *Soil Sci.* **1981**, *131*, 53–55. [CrossRef]
7. Postma, D. Concentration of Mn and separation from Fe in sediments—I. Kinetics and stoichiometry of the reaction between birnessite and dissolved Fe(II) at 10 °C. *Geochim. Et Cosmochim. Acta* **1985**, *49*, 1023–1033. [CrossRef]
8. Villinski, J.E.; O'DAy, P.A.; Corley, T.L.; Conklin, M.H. In situ spectroscopic and solution analyses of the reductive dissolution of MnO_2 by Fe(II). *Environ. Sci. Technol.* **2001**, *35*, 1157–1163. [CrossRef] [PubMed]
9. Villinski, J.E.; Saiers, J.E.; Conklin, M.H. The effects of reaction-product formation on the reductive dissolution of MnO_2 by Fe(II). *Environ. Sci. Technol.* **2003**, *37*, 5589–5596. [CrossRef] [PubMed]
10. Siebecker, M.; Madison, A.S.; Luther, G.W., III. Reduction kinetics of polymeric (soluble) manganese (IV) oxide (MnO_2) by ferrous iron (Fe^{2+}). *Aquat. Geochem.* **2015**, *21*, 143–158. [CrossRef]
11. Burdige, D.J.; Dhakar, S.P.; Nealson, K.H. Effects of manganese oxide mineralogy on microbial and chemical manganese reduction. *Geomicrobiol. J.* **1992**, *10*, 27–48. [CrossRef]
12. Krishnamurti, G.; Huang, P. The catalytic role of birnessite in the transformation of iron. *Can. J. Soil Sci.* **1987**, *67*, 533–543. [CrossRef]
13. Gao, T.; Shen, Y.; Jia, Z.; Qiu, G.; Liu, F.; Zhang, Y.; Feng, X.; Cai, C. Interaction mechanisms and kinetics of ferrous ion and hexagonal birnessite in aqueous systems. *Geochem. Trans.* **2015**, *16*, 16. [CrossRef] [PubMed]
14. Wu, Y.; Kukkadapu, R.K.; Livi, K.J.T.; Xu, W.; Li, W.; Sparks, D.L. Iron and arsenic speciation during as(III) oxidation by manganese oxides in the presence of Fe(II): Molecular-level characterization using XAFS, mossbauer, and TEM analysis. *ACS Earth Space Chem.* **2018**, *2*, 256–268. [CrossRef]
15. Mock, R.P.; Schaefer, M.V.; Pacheco, J.L.; Lake, L.; Lee, I.; Ying, S.C. Influence of Fe(II) on arsenic(III) oxidation by birnessite in diffusion-limited systems. *ACS Earth Space Chem.* **2019**, *3*, 550–561. [CrossRef]
16. Aiken, M.L.; Abernathy, M.J.; Schaefer, M.V.; Lee, I.; Ying, S.C. Inhibition of chromium(III) oxidation through manganese(IV) oxide passivation and iron(II) abiotic reduction. *ACS Earth Space Chem.* **2023**, *7*, 2327–2338. [CrossRef]
17. Limmer, M.A.; Linam, F.A.; Evans, A.E.; Seyfferth, A.L. Unraveling the mechanisms of Fe oxidation and Mn reduction on Mn indicators of reduction in soil (IRIS) films. *Environ. Sci. Technol.* **2023**, *57*, 6530–6539. [CrossRef] [PubMed]
18. Manceau, A.; Tamura, N.; Celestre, R.S.; MacDowell, A.A.; Geoffroy, N.; Sposito, G.; Padmore, H.A. Molecular-scale speciation of Zn and Ni in soil ferromanganese nodules from loess soils of the Mississippi Basin. *Environ. Sci. Technol.* **2003**, *37*, 75–80. [CrossRef] [PubMed]
19. Villalobos, M.; Toner, B.; Bargar, J.; Sposito, G. Characterization of the manganese oxide produced by Pseudomonas putida strain MnB1. *Geochim. Et Cosmochim. Acta* **2003**, *67*, 2649–2662. [CrossRef]
20. Villalobos, M.; Lanson, B.; Manceau, A.; Toner, B.; Sposito, G. Structural model for the biogenic Mn oxide produced by Pseudomonas putida. *Am. Mineral.* **2006**, *91*, 489–502. [CrossRef]
21. Thamdrup, B. Bacterial Manganese and Iron Reduction in Aquatic Sediments, in Advances. In *Microbial Ecology*; Springer: Berlin/Heidelberg, Germany, 2000; pp. 41–84.
22. Chin, Y.P.; Traina, S.J.; Swank, C.R.; Backhus, D. Abundance and properties of dissolved organic matter in pore waters of a freshwater wetland. *Limnol. Oceanogr.* **1998**, *43*, 1287–1296. [CrossRef]
23. Luther, G.W., III; E Kostka, J.; Church, T.M.; Sulzberger, B.; Stumm, W. Seasonal iron cycling in the salt-marsh sedimentary environment: The importance of ligand complexes with Fe(II) and Fe(III) in the dissolution of Fe(III) minerals and pyrite, respectively. *Mar. Chem.* **1992**, *40*, 81–103. [CrossRef]
24. Luther, G.W., III. *Inorganic Chemistry for Geochemistry and Environmental Sciences: Fundamentals and Applications*; John Wiley & Sons: New York, NY, USA, 2016.
25. Ballesteros, M.A.C.; Rueda, E.H.; Blesa, M.A. The influence of iron (II) and (III) on the kinetics of goethite dissolution by EDTA. *J. Colloid Interface Sci.* **1998**, *201*, 13–19. [CrossRef]

26. Buerge, I.J.; Hug, S.J. Influence of organic ligands on chromium(VI) reduction by iron(II). *Environ. Sci. Technol.* **1998**, *32*, 2092–2099. [CrossRef]
27. Masscheleyn, P.H.; Delaune, R.D.; Patrick, W.H., Jr. Effect of redox potential and pH on arsenic speciation and solubility in a contaminated soil. *Environ. Sci. Technol.* **1991**, *25*, 1414–1419. [CrossRef]
28. Strobel, B.W. Influence of vegetation on low-molecular-weight carboxylic acids in soil solution—A review. *Geoderma* **2001**, *99*, 169–198. [CrossRef]
29. McKenzie, R. The synthesis of birnessite, cryptomelane, and some other oxides and hydroxides of manganese. *Mineral. Mag.* **1971**, *38*, 493–502. [CrossRef]
30. Stookey, L.L. Ferrozine—A new spectrophotometric reagent for iron. *Anal. Chem.* **1970**, *42*, 779–781. [CrossRef]
31. Elzinga, E.J. Reductive transformation of birnessite by aqueous Mn(II). *Environ. Sci. Technol.* **2011**, *45*, 6366–6372. [CrossRef] [PubMed]
32. Sparks, D.L. Kinetics and Mechanisms of Chemical Reactions at the Soil Mineral/water Interface. In *Soil Physical Chemistry*; CRC press: Boca Raton, FL, USA, 2018; pp. 135–192.
33. Scheinost, A.C.; Ford, R.G.; Sparks, D.L. The role of Al in the formation of secondary Ni precipitates on pyrophyllite, gibbsite, talc, and amorphous silica: A DRS study. *Geochim. Et Cosmochim. Acta* **1999**, *63*, 3193–3203. [CrossRef]
34. Torrent, J.; Barrón, V. Diffuse reflectance spectroscopy. In *Methods of Soil Analysis Part 5—Mineralogical Methods*; Soil Science Society of America: Madison, WI, USA, 2008; Volume 5, pp. 367–385.
35. Villalobos, M.; Escobar-Quiroz, I.N.; Salazar-Camacho, C. The influence of particle size and structure on the sorption and oxidation behavior of birnessite: I. Adsorption of As(V) and oxidation of As(III). *Geochim. Et Cosmochim. Acta* **2014**, *125*, 564–581. [CrossRef]
36. Sparks, D.L.; Singh, B.; Siebecker, M.G. *Environmental Soil Chemistry*; Elsevier: San Diego, CA, USA, 2022.
37. Wang, Y.; Benkaddour, S.; Marafatto, F.F.; Peña, J. Diffusion-and pH-dependent reactivity of layer-type MnO_2: Reactions at particle edges versus vacancy sites. *Environ. Sci. Technol.* **2018**, *52*, 3476–3485. [CrossRef] [PubMed]
38. Luther, G.W., III. Manganese(II) oxidation and Mn(IV) reduction in the environment—Two one-electron transfer steps versus a single two-electron step. *Geomicrobiol. J.* **2005**, *22*, 195–203. [CrossRef]
39. Luther, G.W., III; de Chanvalon, A.T.; Oldham, V.E.; Estes, E.R.; Tebo, B.M.; Madison, A.S. Reduction of manganese oxides: Thermodynamic, kinetic and mechanistic considerations for one-versus two-electron transfer steps. *Aquat. Geochem.* **2018**, *24*, 257–277. [CrossRef]
40. Geschwind, S.; Kisliuk, P.; Klein, M.P.; Remeika, J.P.; Wood, D.L. Sharp-line fluorescence, electron paramagnetic resonance, and thermoluminescence of Mn^{4+} in α-Al_2O_3. *Phys. Rev.* **1962**, *126*, 1684. [CrossRef]
41. Sherman, D.M.; Vergo, N. Optimal spectrum, site occupancy, and oxidation state of Mn in montmorillonite. *Am. Mineral.* **1988**, *73*, 140–144.
42. Golden, D.; Chen, C.; Dixon, J.; Tokashiki, Y. Pseudomorphic replacement of manganese oxides by iron oxide minerals. *Geoderma* **1988**, *42*, 199–211. [CrossRef]
43. Kopf, S.H.; Henny, C.; Newman, D.K. Ligand-enhanced abiotic iron oxidation and the effects of chemical versus biological iron cycling in anoxic environments. *Environ. Sci. Technol.* **2013**, *47*, 2602–2611. [CrossRef] [PubMed]
44. Hudson, J.M.; Luther, G.W., III; Chin, Y.-P. Assessing Iron Complexation by Dissolved Organic Matter Using Mediated Electrochemical Oxidation. *ACS Earth Space Chem.* **2024**, *8*, 1810–1819. [CrossRef]
45. Madison, A.S.; Tebo, B.M.; Mucci, A.; Sundby, B.; Luther, G.W. Abundant porewater Mn(III) is a major component of the sedimentary redox system. *Science* **2013**, *341*, 875–878. [CrossRef] [PubMed]
46. Pyzola, S.; Dhakal, P.; Coyne, M.; Grove, J.; Vandiviere, M.; Matocha, C. Transformation of organic matter under anoxic conditions in soils. *Sci. Total Environ.* **2025**, *970*, 178899. [CrossRef] [PubMed]

Disclaimer/Publisher's Note: The statements, opinions and data contained in all publications are solely those of the individual author(s) and contributor(s) and not of MDPI and/or the editor(s). MDPI and/or the editor(s) disclaim responsibility for any injury to people or property resulting from any ideas, methods, instructions or products referred to in the content.